EXPERIMENTAL INVESTIGATION OF UNCONFINED SPHERICAL AND CYLINDRICAL FLAME PROPAGATION IN HYDROGEN-AIR MIXTURES

Grune, J. [1], Sempert, K. [1], Kuznetsov, M[2]. and Jordan, T.[2]
[1]Pro-Science GmbH, Parkstrasse 9, Ettlingen, 76275, Germany,
[2]Karlsruhe Institute of Technology, Kaiserstrasse 12, Karlsruhe, 76131, Germany

*E-mail: grune@pro-science.de

**Corresponding author: grune@pro-science.de*

ABSTRACT

This paper presents results of experimental investigations on spherical and cylindrical flame propagation in pre-mixed H_2/air-mixtures in unconfined and semi-confined geometries. The experiments were performed in a facility consisting of two transparent solid walls with 1 m^2 area and four weak side walls made from thin plastic film. The gap size between the solid walls was varied stepwise from thin layer geometry (6 mm) to cube geometry (1 m). A wide range of H_2/air-mixtures with volumetric hydrogen concentrations from 10 % to 45 % H_2 was ignited between the transparent solid walls. The propagating flame front and its structure was observed with a large scale high speed shadow system. Results of spherical and cylindrical flame propagation up to a radius of 0.5 m were analyzed. The presented spherical burning velocity model is used to discuss the self-acceleration phenomena in unconfined and unobstructed pre-mixed H_2/air flames.

1.0 INTRODUCTION

The understanding of flame propagation in pre-mixed H_2/air mixtures in unconfined and semiconfined geometries is very important for the estimation of hazard potential in free field and large scale industrial applications. In case of an accidental formation of a large flammable H_2/air cloud and a late weak ignition the mixture burns in the early stage undisturbed in an unconfined spherical or semiconfined mode.

It is well known that H_2/air flames are influenced by complex flame instabilities which effect the flame velocity and the resulting pressure loads. First a freely propagating spherical H_2/air flame burns driven by the ignition source - for a weak ignition energy the effected flame radius is in a range of mm - then the flame burns in a quasi-laminar mode for a few further mm. The laminar burning velocity will be influenced by the stretch rate gained due to the narrow radius. In the next step the flame front turns into a cellular flame structure which increases the flame surface and thereby the burning rate. This effect results in a self-accelerating flame propagation. Sooner or later, depending on the size of the burnable mixture or a confinement the flame will be influenced strongly by the interaction with walls and the flame propagation loses the unconfined nature.

The general hydrodynamic instability which occurs in all flames is generated by the Darrieuse-Landau instability [1,2], which has been extensively studied for spherical-flame propagation [3].

Gostintsev et al. [4,5] suggested that the sustained acceleration is a result of cell splitting, which generates fractal structures of the flame surface and proposed a flame radius (R) time (t) dependence:

$$R = R1 + A\, t^{(3/2)} \qquad (1)$$

Here A and R1 are empirical constants. This basic fractal theory was reformulated [6] and the relation between visible flame velocity (U_{vis}) and flame radius (R) was expressed as:

$$U_{vis} / S_L = (R/R_0)^{\beta} \qquad (2)$$

where S_L is the planar laminar burning velocity of the mixture, R_0 is the critical radius of onset of instability, and β is a fractal excess that can be obtained experimentally. In [7] this relation was applied to spherical-flame propagation of lean H_2/air mixtures. Values for the important critical radius R_0 for the onset of instability were given from 18 mm (12.3 % H_2) up to 30 mm (19.2 % H_2).

Goal of this work is the experimental investigation of the spherical and cylindrical flame propagation of H_2/air mixtures under unconfined conditions. Therefore, experiments in a 1 m^3 cube volume with center ignition and spherical flame propagation were performed. The undisturbed spherical flame propagation is suitable to observe the nature of the visible flame propagation, where only instability effects generated by the flame itself take place. This set-up allows to study the basic natural flame evolution behaviour without influence from interactions with wall structures. Ignition with subsequent undisturbed spherical flame propagation is very unlikely in real accident scenarios. Usually ignition sources are associated with solid objects. This more realistic circumstance was simulated by a cylindrical flame propagation which represents semi-confined conditions. Experiments with cylindrical flame propagation were performed with 1 m^2 area and gap sizes from 6 to 250 mm. For a proper optical flame observation the combustion chambers consist of two solid transparent 1 m^2 plates and four soft and weak walls. Based on the simple relation for spherical flame propagation (3), the visible flame speed V_{vis} is the product of the expansion ratio σ and its characteristic burning velocity S:

$$V_{vis} = \sigma S \qquad (3)$$

Both, σ and S, are thermodynamic properties of the mixture. The planar laminar burning velocity S_L, which is a basic propagation velocity, typically deviates from the initial propagation velocity of a spherical flame [8]. The fundamental burning speed in general does not occur in realistic premixed H_2/air combustion scenarios. The self-turbulizing spherical flame propagation velocity along the flame radius V_{vis} (R) should be describable as:

$$V_{vis}(R) = B\, R\, \sigma\, S_{(sph)} \qquad (4)$$

where σ is the ratio of the gas expansion, R is the radius of the flame front, $S_{(sph)}$ is a characteristic spherical burning velocity for undisturbed spherical flame propagation and the acceleration factor B is a constant or a function of R. In this study the characteristic spherical burning velocity $S_{(sph)}$ and acceleration factor B will be determined experimentally. The results are applied to available large scale spherical H_2/air flame propagation data [4,7,9] and furthermore to the performed cylindrical H_2/air flame propagation experiments.

2.0 EXPERIMENTAL SET-UP

The experiments were performed at the KIT hydrogen test site HYKA in a 160 m^3 test camber. The facility consists of two transparent solid walls with 1 m^2 area (a) and four weak side walls made from thin plastic film sheets (10 µm thickness). Fig 1 left shows the configuration for spherical-flame propagation were the gap size between the two transparent solid walls is 1 m and the combustion chamber is a cube. In the center of Fig. 1 the configuration for cylindrical flame propagation is illustrated, where the solid plates are shifted together. The pre mixed H_2/air mixture is provided by mass flow controllers and is injected from several positions at the top of the compartment (b). The gas exhaust (c) is located in each corner on the ground level of the compartment. The H_2-concentration in the exhaust flow is monitored continuously. If the hydrogen concentrations of the feed and exhaust flow are equal it is assumed that the volume is completely filled with the fuel mixture. The point of ignition is located in the center of the compartment using thin electrodes mounted perpendicularly to the transparent solid walls. The ignition is initiated by a weak spark (< 100 mJ). To monitor the overpressure in the compartment an acoustic pressure gauge (PCB Type A102 – range: 720 mbar) is connected via a tube (di = 2 mm) to the soft ground of the compartment, located in a distance of 0.5 m from the ignition point in all configurations.

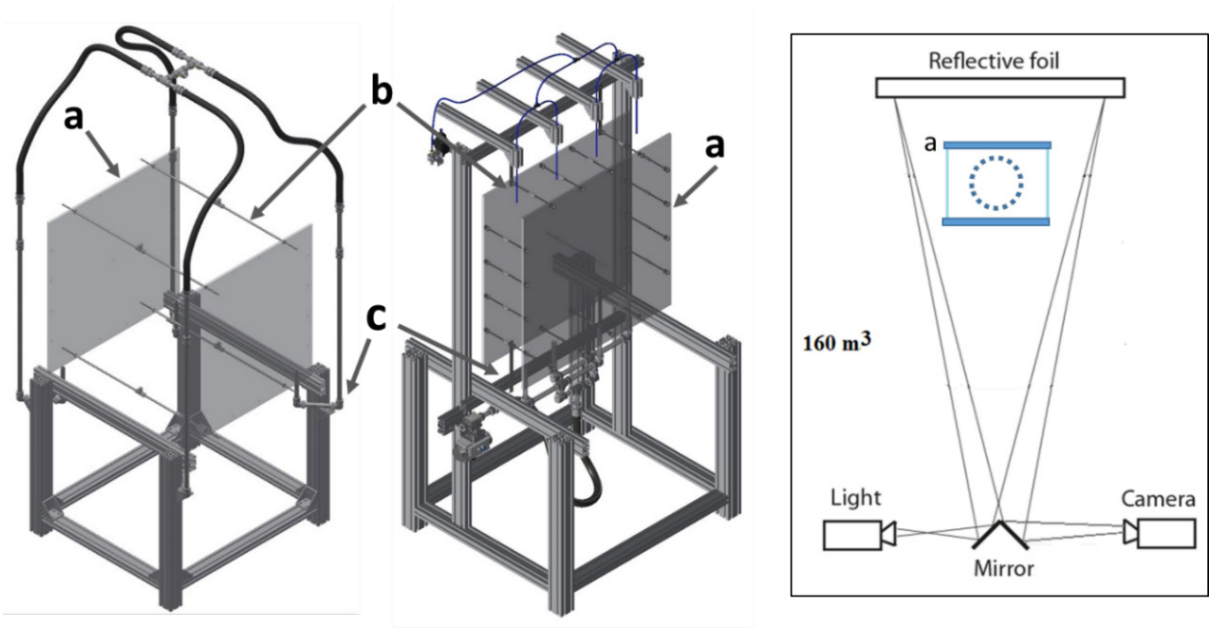

Fig 1: Left, test facility in configuration for spherical flame propagation. Middle, test facility in configuration for cylindrical flame propagation. Right, top view of the optical set up.

The flame front propagation is measured by using a large scale shadowgraphy set-up for high speed applications. The right part of Fig. 1 sketches a top view of the optical set up installed in the test cell with 160 m^3 free volume. A 100 W point light source produces a conical light beam through the parallel transparent plates. The light beam is reflected on a special reflective foil behind the test facility and returns as a cone to its origin. A mirror is used to capture the reflected light. A high speed camera (Fast Cam SA1) with a frame rate of up to 5000 f/s is used to observe the flame front propagation over an area of 1 m^2. Fig. 2 shows two combustion test compartments equipped with the soft wall sheets (thin film). On the left side the cube configuration for spherical flame propagation is shown in a view perpendicular to the solid transparent walls. The right picture shows an example (gap size 250 mm) for the configuration for cylindrical flame propagation with prepared soft walls as side view.

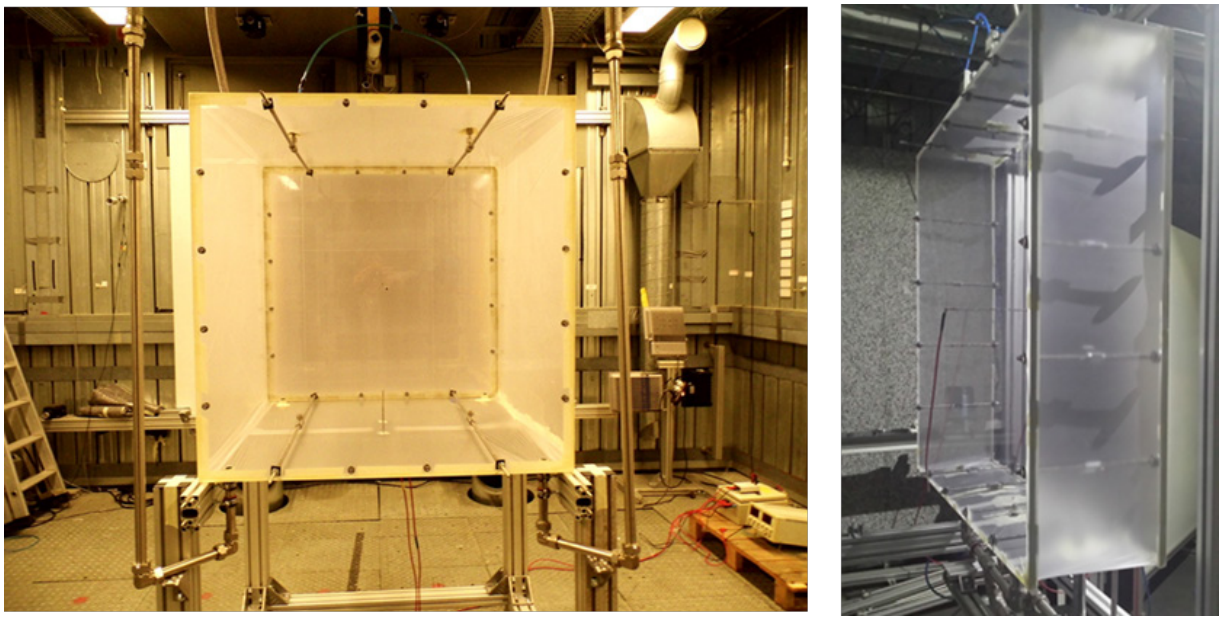

Fig. 2: Combustion test compartments equipped with the soft walls. Left, cube configuration for spherical flame propagation. Right, configuration for cylindrical flame propagation.

2.1 Test Matrix

Tab. 1 contains the test matrix. The investigated H_2-concentration starts from the lean side with 10 % H_2. Smaller concentrations were avoided to exclude strong buoyancy effects. The maximum H_2-concentration on the rich side was 45 % H_2. In the spherical configuration (gap size 1 m) the maximum H_2-concentration was limited to 22 % H_2. The table also shows corresponding values of the expansion ratio σ and the planar laminar flame burning velocity S_L. Furthermore, values for a characteristic spherical burning velocity $S_{(sph)}$ are included.

Tab. 1**:** Summary of test conditions and mixture properties

Fuel concentration	expansion ratio	planar laminar flame burning velocity	spherical burning velocity	spherical configuration gap size	cylindrical configuration gap size	cylindrical configuration gap size	cylindrical configuration gap size	cylindrical configuration gap size	cylindrical configuration gap size	cylindrical configuration gap size
H2 %	σ	SL / (m/s)	$S_{(sph)}$/ m/s	1 m	6 mm	10 mm	22 mm	50 mm	100 mm	250 mm
10	3.54	0.12	0.25		x	x	x		x	x
11	3.77	0.16	0.33	x	x	x	x	x	x	
12	3.99	0.21	0.42	x	x	x	x	x	x	x
13	4.21	0.27	0.53	x	x	x	x		x	
14	4.42	0.34	0.65	x	x	x	x	x	x	x
15	4.63	0.41	0.77		x	x	x		x	
16	4.83	0.49	0.91	x	x	x	x	x	x	x
18	5.23	0.68	1.19	x	x	x	x		x	
20	5.60	0.90	1.47		x	x	x	x	x	x
22	5.97	1.15	1.73	x						
25	6.45	1.54	2.01		x	x	x		x	
30	7.02	2.20	2.11		x	x	x	x	x	x
40	6.60	2.75	1.85		x	x	x	x	x	
45	6.27	2.75	1.85		x	x	x	x	x	x

3.0. RESULTS

3.1 Spherical flame propagation

Fig. 3 shows a representative result of large scale shadowgraphy images for a spherical flame propagation with 14 % H_2 mixture. The left part (A) shows the original snapshot from the high speed movie while the middle part (B) is slightly processed to highlight the complex wrinkled surface of the flame front. The right part (C) illustrates the temporal evolution of the flame front. The total time distance between inner and outer flame front amounts to 16.6 ms, Fig. 3 (C) shows how the characteristic wrinkled structure grows with increasing radius.

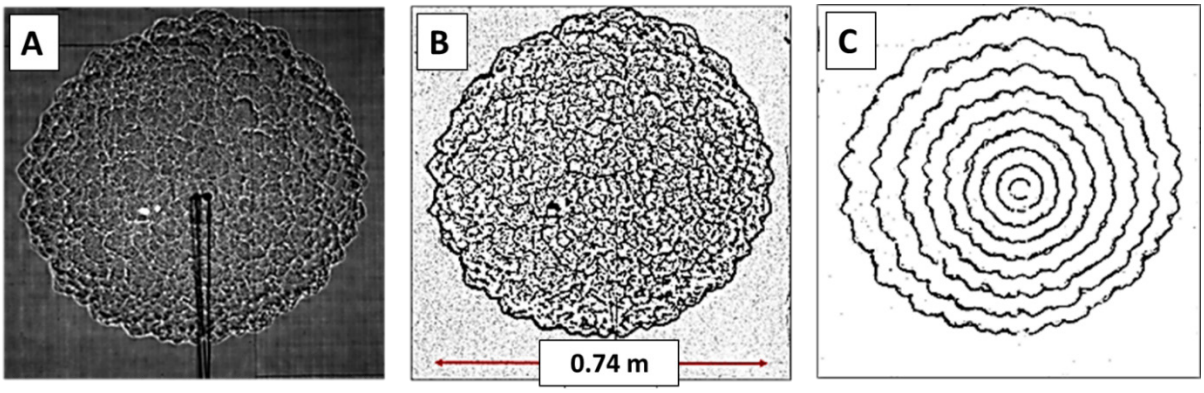

Fig. 3: Example of large scale shadow pictures for spherical flame propagation of a 14 % H_2 mixture.

Fig, 4 left shows exemplarily a radius-time diagram taken from the high speed movie (14 % H_2). Here the propagation direction of the spherical flame front is in horizontal direction. The right side of Fig. 4 shows the corresponding overpressure history in the test compartment. When the flame radius reaches

a value of 0.38 m an overpressure of only 4.5 mbar was measured inside the compartment. The reason is the large area of the four 1 m^2 soft walls segments. These segments are able to blow up in a hemispherical manner to increase the volume of the compartment strongly at very low pressure (< 5 mbar). For all spherical configuration experiments the maximum overpressure was < 10 mbar reached at a flame radius of 0.4 m. Due to the low overpressure developed by the transient flame in the compartment it is assumed that the experimental conditions are very close to unconfined.

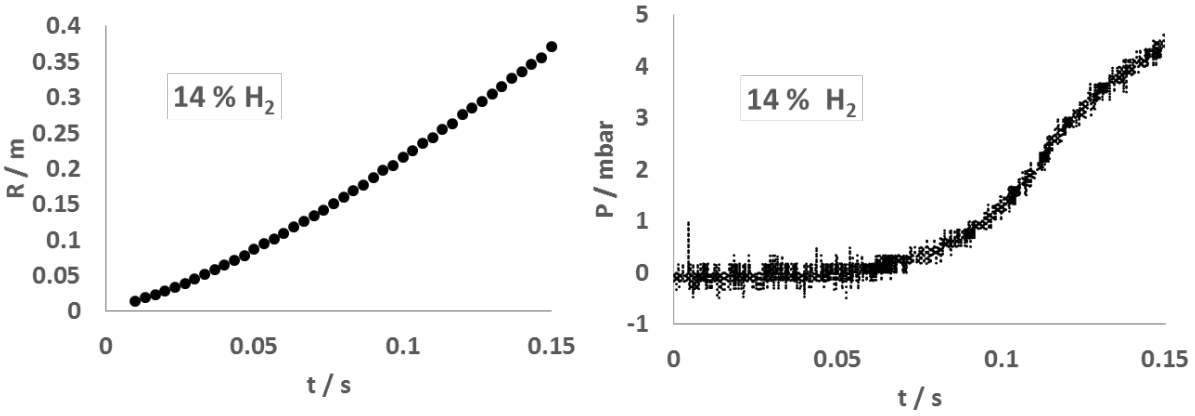

Fig. 4: Example of the spherical flame propagation (14 % H_2) as radius/time diagram (left) and the corresponding history of overpressure in the test compartment (right).

Radius-time data was transferred into radius-velocity data by appropriate difference schemes. Even though no significant flame oscillation was monitored in the spherical flame propagation experiments, large scattering of local velocities was observed.

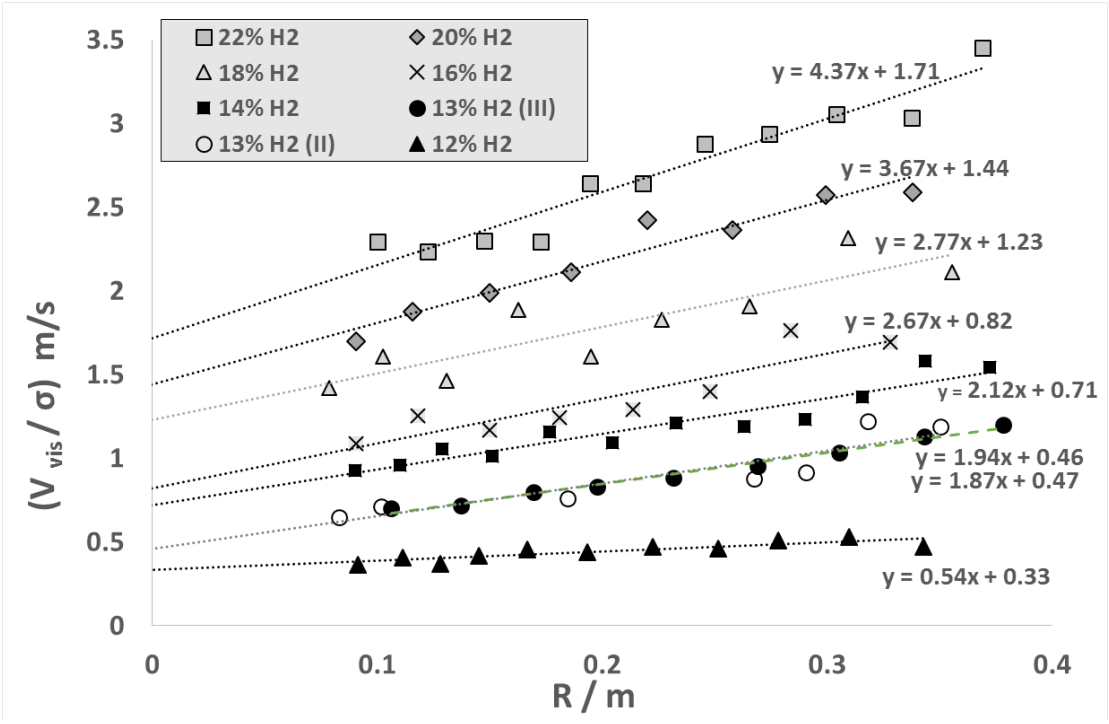

Fig. 5: Visible flame speed in spherical flame propagation.

In the velocity diagram (Fig. 5) a limited amount of data points is used to illustrate the local average velocities of the flame front. Fig. 5 shows the velocities of the spherical flame front propagation for

different mixtures along the radius in horizontal direction. The velocity is scaled as the measured visible flame velocity V_{vis} divided by the mixture specific ratio of the gas expansion σ. All concentration curves show fairly linear dependence, this indicates a linear flame acceleration with increasing radius. In the first 0.08 cm no data points are plotted, as in this zone the flame is influenced by the ignition itself and by the effects of the narrow radius (see Fig. 7). However, the linear fit of each radius-velocity curve yields a discrete value for the flame velocity at R = 0. These values define the H_2-concentration specific spherical burning velocity $S_{(sph)}$.

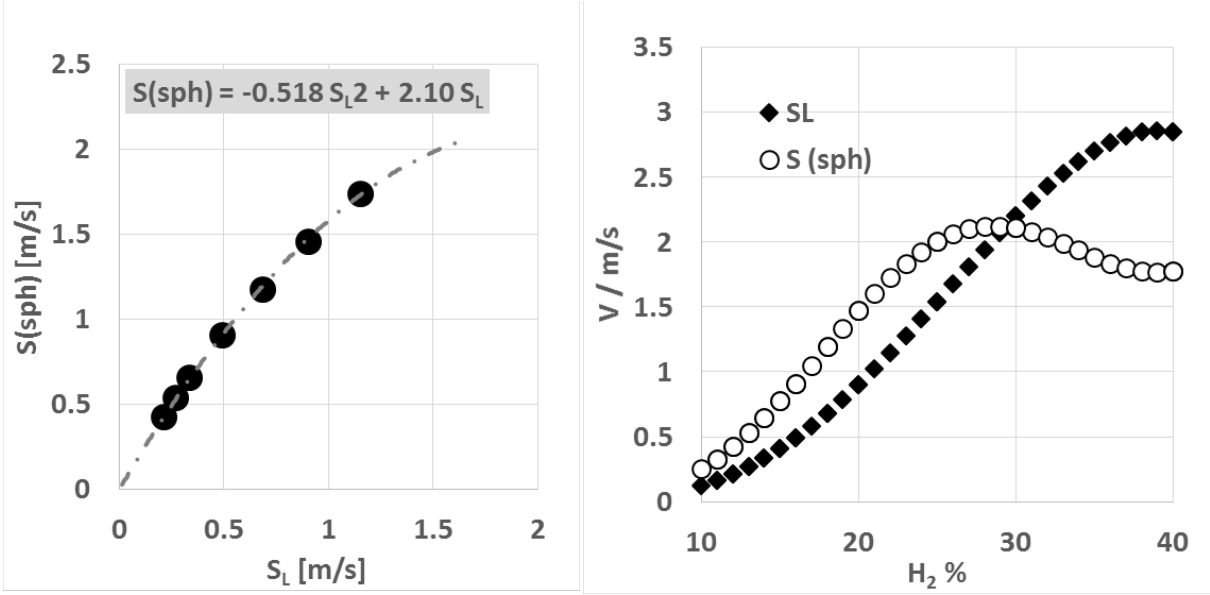

Fig. 6: Left, planar laminar burning velocity S_L versus spherical burning velocity $S_{(sph)}$. Right, planar laminar burning velocity S_L and spherical burning velocity $S_{(sph)}$ versus H_2 concentration.

Fig. 6 illustrates the dependencies of the planar laminar burning velocity S_L and the spherical burning velocity $S_{(sph)}$. The left side shows a quadratic relation of the planar laminar burning velocity S_L and the experimentally determined spherical burning velocity $S_{(sph)}$. With the correlation given in the left part of Fig. 6 the spherical burning velocity $S_{(sph)}$ can be extrapolated to a wider range of H_2-concentrations. Fig. 6 right compares the planar laminar burning velocity S_L with the spherical burning velocity $S_{(sph)}$ depending on the H_2-concentrations. The data show that for lean H_2/air mixtures (range 10 to 16 %) the $S_{(sph)}$ is about two times higher as S_L. Such mixtures are very sensitive to flame instabilities. At 20 % H_2 $S_{(sph)}$ is about 1.5 times higher than S_L while at stoichiometric conditions both values were equal. In the region of rich H_2/air mixtures the spherical burning velocity $S_{(sph)}$ is smaller than the planar laminar burning velocity S_L. The explanation for this behaviour is that the flame front of rich H_2/air mixtures is relatively smooth compared to the heavily wrinkled surface of lean H_2/air mixtures.

Fig. 7 shows radius-velocity diagrams for the spherical flame propagation experiments in upward and downward direction. The visible flame velocity divided by the expansion ratio σ of the mixture is now scaled as spherical burning velocity $S_{(sph)}$ (Eq. 4). All curves collapse together and represent a fairly linear growing with increasing radius. This indicates a linear flame acceleration of the flame front with a constant acceleration factor B = (2.6 R +1) for all mixtures investigated. The plots show that the flame velocity of the base values $S_{(sph)}$ = 1 will be reached after a short distance which is shorter than 0.05 m and mostly much shorter. The left diagram (upward propagation) shows better results while in the right diagram (downward propagation) slight buoyancy effects for the leanest investigated mixtures are visible. But nevertheless in all experiments an evenly sphere body of the flame front was observed and the flame front propagation can be linked quantitatively with the Eq. 5:

$$V_{vis}(R) = (2.6\,R + 1)\,\sigma\,S_{(sph)} \qquad (5)$$

where σ is the ratio of the gas expansion, R is the radius of the flame front and $S_{(sph)}$ is a characteristic spherical burning velocity for undisturbed spherical flame propagation., The value 2.6 is a constant acceleration factor.

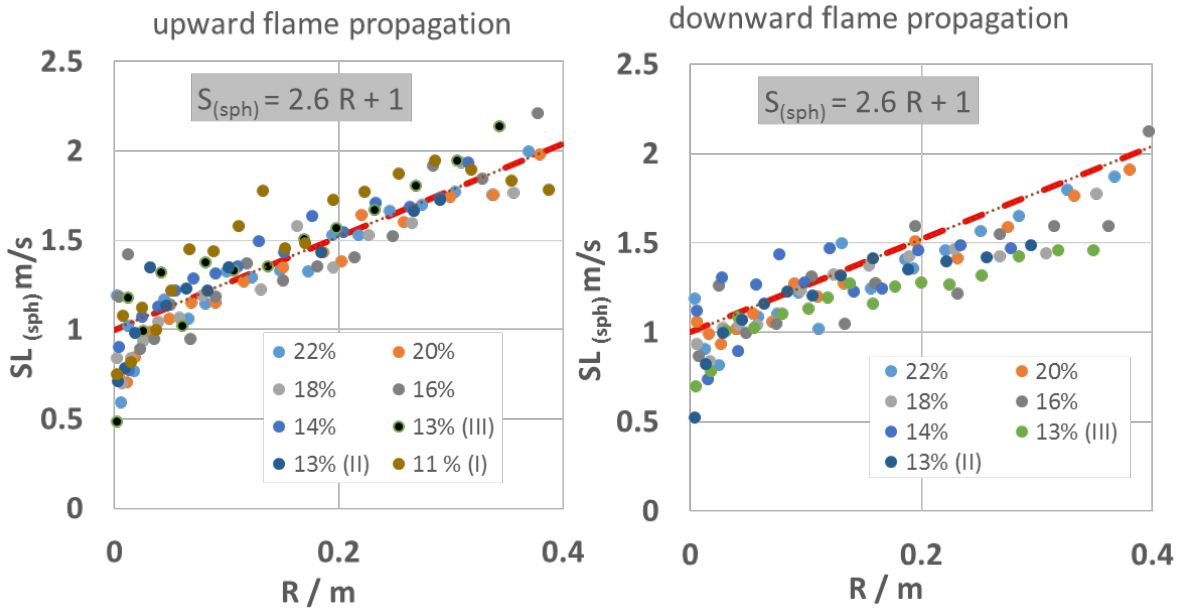

Fig. 7: Flame speed versus radius in spherical flame propagation expressed as spherical burning velocity $S_{(sph)}$.

3.2 Cylindrical flame propagation

The experiments regarding the cylindrical flame propagation were performed in the same way as the experiments for the spherical flame propagation. The only difference is the gap size between the solid transparent plates. The large scale shadow system was able to capture the flame front for lean H_2 mixtures inside the smallest investigated gap size of 6 mm. Fig. 8 shows representative results of shadowgraphy applied to a 13 % H_2 mixture for different gap sizes. All snapshots were taken at the same time after ignition and show the upper part of the flames, which all have a typical radius of ~ 0.2 m. The flame front structure for the 6 mm gap looks quite different compared to the structures for larger gap sizes.

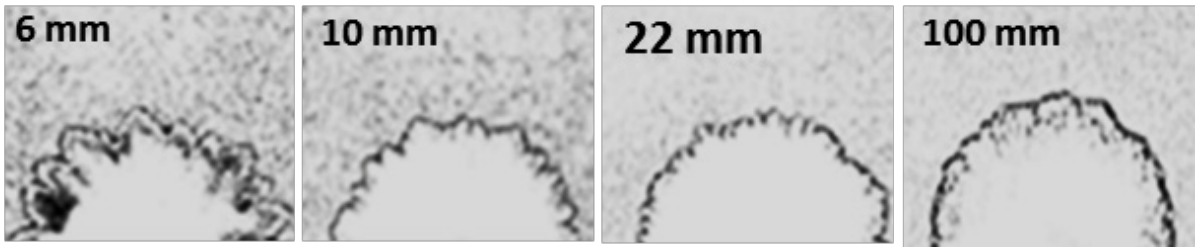

Fig. 8: Examples of large scale shadowgraphs for cylindrical flame propagation with 13 % H_2 mixture for different gap sizes.

Fig. 9 shows shadowgraphs of the cylindrical flame propagation of a 14 % H_2 mixture in a 10 mm gap. On the top the cylindrical flame front propagation is illustrated as distance-time diagram. The flame propagation is up- and downwards. After the ignition the flame accelerates and reaches a region of nearly constant speed. Afterwards the flame velocity starts to decay. The flame propagation is very symmetrical

as shown in the shadow picture series in Fig. 9 in the middle, the structure of the cylindrical flame front in the 10 mm gap looks very similar to the spherical flame front presented in Fig. 3.

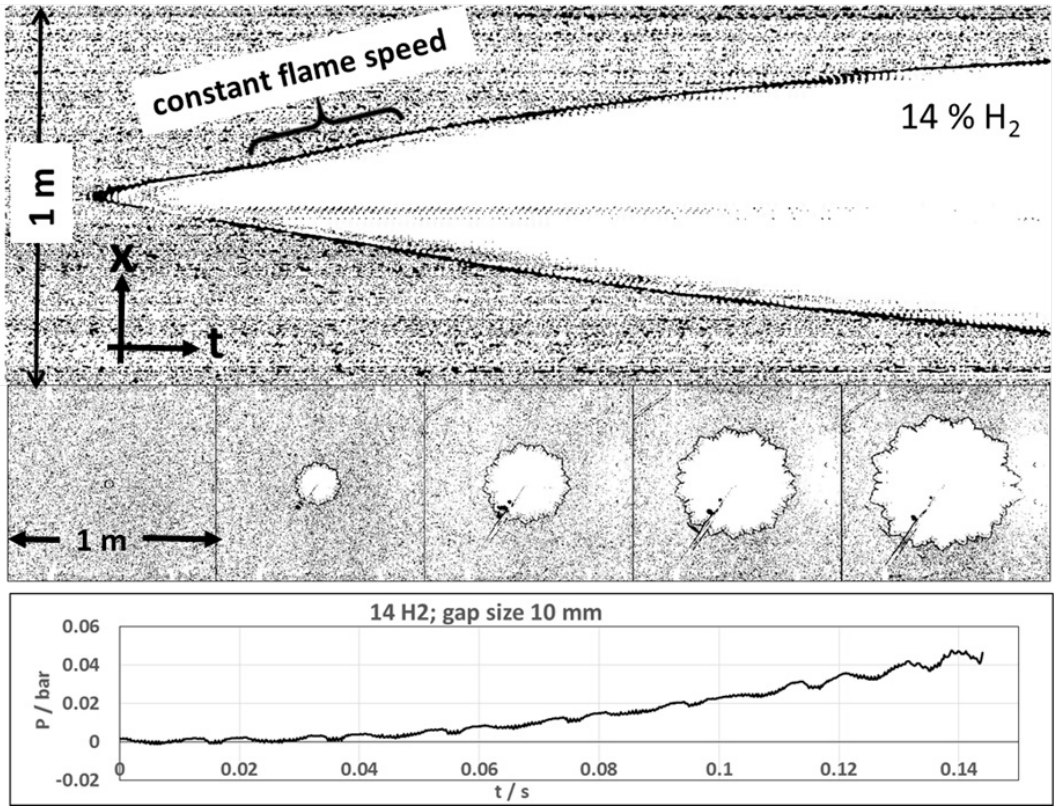

Fig. 9: Example of large scale shadowgraphs for cylindrical flame propagation of a 14 % H2 mixture in a 10 mm gap and the corresponding overpressure in the test compartment.

The lower part of Fig. 9 shows the corresponding pressure history in the compartment measured in 0.5 m distance to the ignition point. In this example an overpressure of 50 mbar is reached during the cylindrical flame propagation. Compared to the spherical flame propagation for the same H_2-concentration (Fig. 4) this value is 10 times higher for the cylindrical configuration. In general the measured pressure in the cylindrical flame propagation is much higher than in the spherical experiments. One reason is the lower ratio of unburned to burned gas in the cylindrical configuration and secondly the area of the soft walls. Due to the small area of the thin plastic film, the film is less flexible and does not allow similar volume increases for such a low pressure compared to the spherical configuration. It was observed that the enclosure is strong enough to create acoustic flame instabilities which finally lead to an oscillating flame propagation as described in [10]. The analyses of the values of the nearly constant flame velocity for the cylindrical flame propagation is shown in Fig. 10. The left side shows the measured average visible flame velocity in up- and downward and a horizontal direction, scaled by the expansion value σ and corresponding planar laminar flame burning velocity S_L. Again, the influence of the gap sizes is remarkably low, and all points show a typical trend. Between 10 % and 20 % H_2 the scaled velocity reaches values which are more than two times higher than S_L, with a clear maximum of about 2.3 for concentrations close to 15 % H_2. Between 20 % and 30 % H_2 the velocity decays to a value of ~ 1.3 S_L. The typical trend reflects the sensitivity of flame instabilities for different H_2/air mixtures. The right side of Fig. 10 shows examples of the visible flame velocity for upward, downward and sideward propagation for the investigated gap sizes. The cylindrical flame propagation is very symmetrical and the difference of the measured flame velocity is low for the investigated gap sizes. An exemption is the gap size of 250 mm, for this gap size the analyzed constant flame speed is much higher than for smaller sizes. Here the flame burns up to a radius of 0.125 m as spherical flame and later in time in cylindrical form. It can be assumed, that the flame front does not reach a real cylindrical form in

the short distance. However, the results of the flame velocity with 250 mm gap size shows the same typical trend only at higher values.

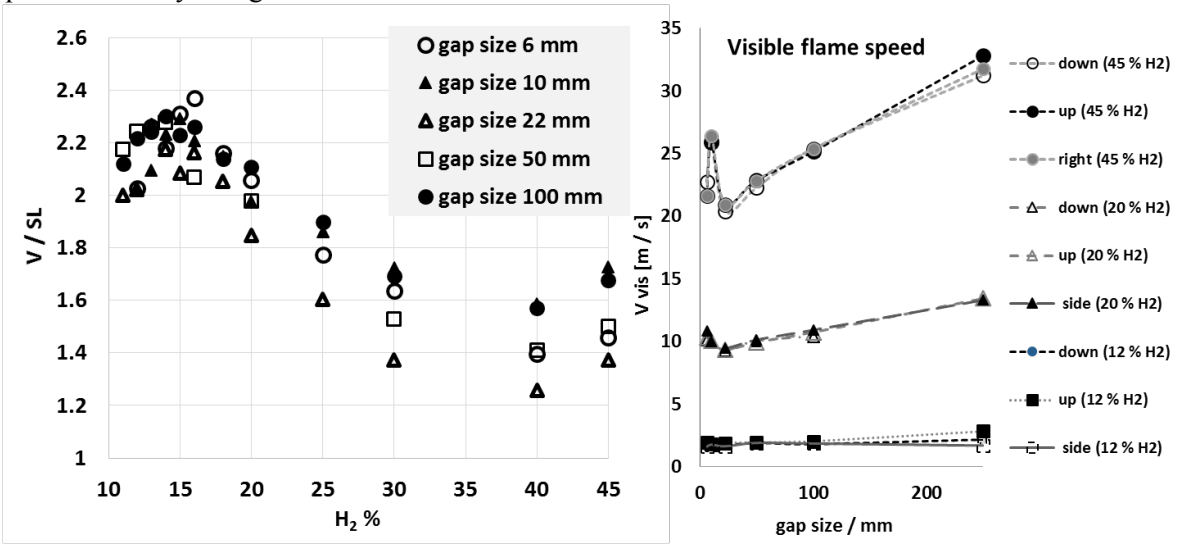

Fig. 10: Left, measured and scaled average flame velocity of cylindrical flame propagation. Right, examples of the visible flame velocity for up-, down- and side-wards cylindrical flame propagation.

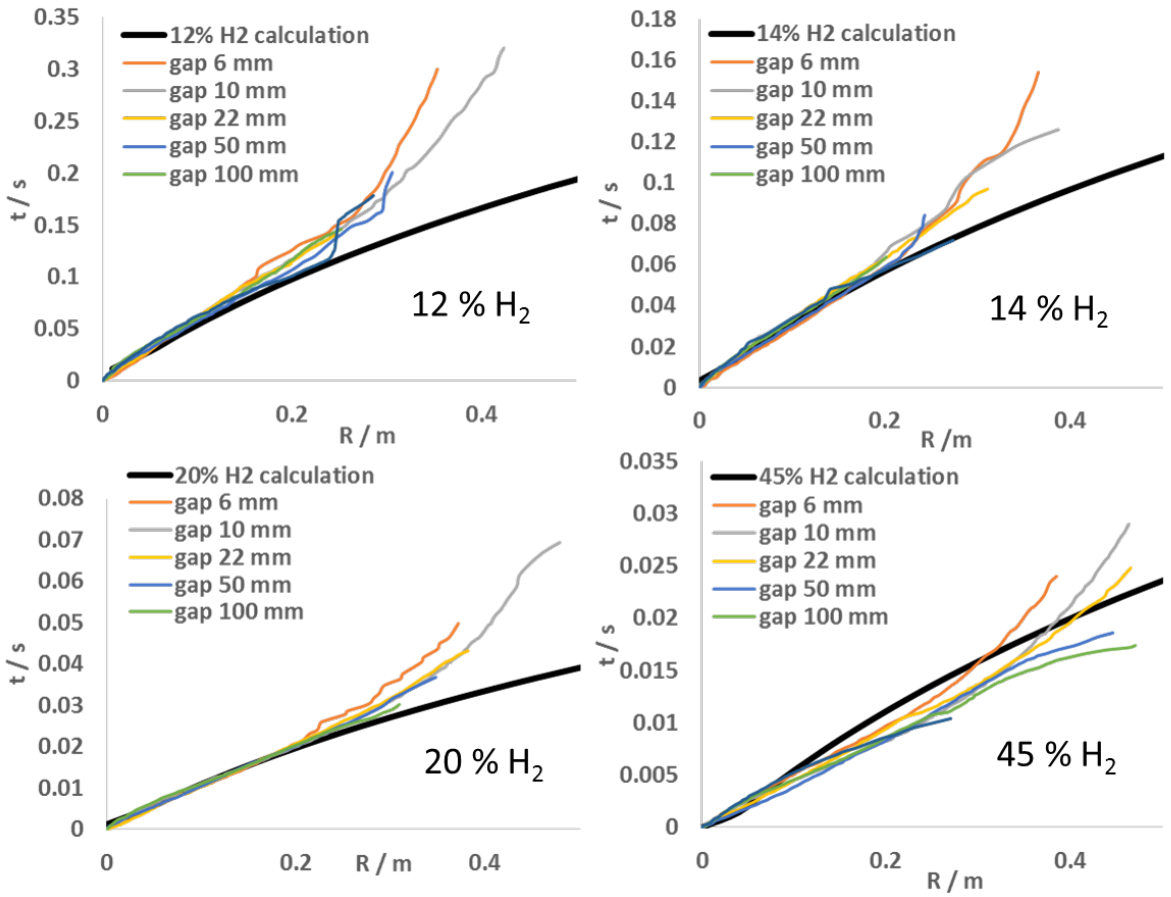

Fig. 11: Examples of radius time curves of the cylindrical flame propagation for different H_2-concentrations and the investigated gap sizes up to 100 mm compared with calculated data (Eq. 5).

Fig. 11 shows examples of radius time curves of the cylindrical flame propagation for different H_2-concentrations and the investigated gap sizes up to 100 mm. Evidently the radius time lines are nearly

identical for the first 0.2 m, independent of the gap size. Beyond 0.2 m the radius time curves start to deviate. Additionally in Fig. 11 data is plotted, which was determined using Eq. 5. Surprisingly the simple model of (Eq. 5), which has been derived from spherical flame propagation, is also able to describe the cylindrical flame propagation up to the critical radius of 0.2 m. The agreement up to this radius is very good, only for the highest investigated H_2-concentration of 45 % a significant deviation is observed. For this concentration the measured flame velocities show both, negative as well as positive, flame acceleration after reaching a distance slightly smaller than 0.2 m. For all other investigated H_2-concentrations the flame velocities then decay. It is assumed that after the critical radius another strong effect influences the flame propagation. Fig. 12 shows two examples of measured radius time curves and the data calculated with Eq. 5 together with the pressure history in the compartment. It is visible that the calculation and the experimental values fit exactly up to the point when the overpressure starts to rise. The level of this overpressure is in a range of 10 mbar for all experiments. It is assumed that the flame loses the unconfined mode at this point. Overpressure and acoustic effects reflected from the soft walls dominate the further flame propagation. In the experiments with spherical flame propagation this effect was not observed because the overpressure has not exceeded the 10 mbar level.

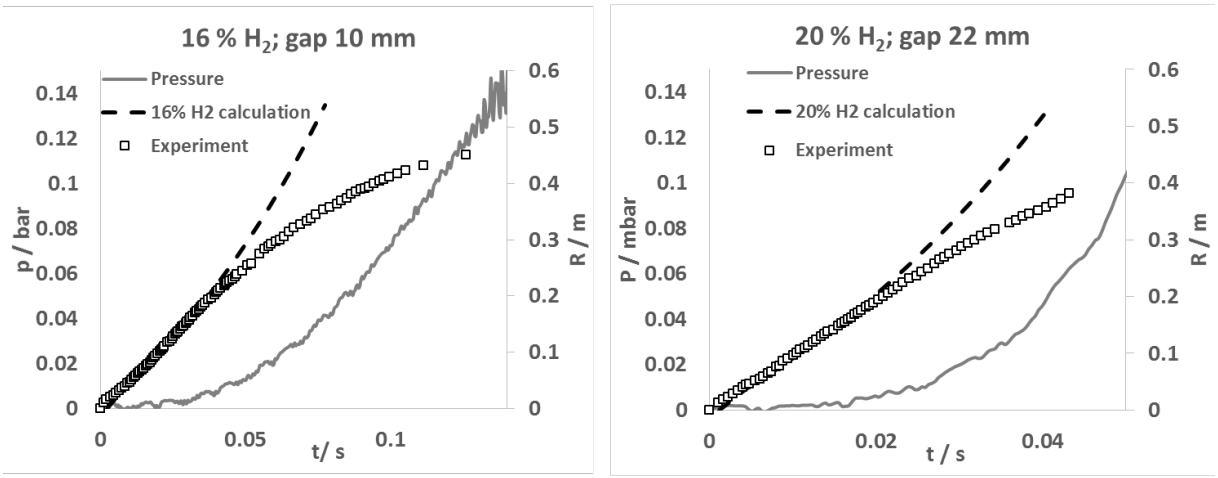

Fig. 12: Examples of measured radius time curves for cylindrical flame propagation, and the data calculated radius time curves (Eq. 5) and pressure histories in the compartment.

4.0 DISCUSSION

A simple model to determine the unconfined spherical flame propagation for a wide range of H_2/air concentrations has been presented. The model is based on a specific burning velocity $S_{(sph)}$, the expansion coefficient σ and a constant acceleration factor. The model is able to predict cylindrical flame propagations up to a radius of about 0.2 m. At this radius the experimental set-up supported a pressure increase of more than 10 mbar. In particular for the small gap experiments it is very difficult to exclude the feedback of the inevitable side wall closures, made from thin plastic film. To create real unconfined conditions larger scales are necessary so that the flame has sufficient space for evolving without unwanted feedback from any limiting walls. Available experimental data for spherical flame propagation of H_2/air mixtures are very rare. Fig. 13 shows some comparisons, using radius-time diagrams of the model (Eq. 5) with other experimental data. The model shows very good agreement with the data presented in [5]. More remarkable is the comparison with experimental data from [4] where larger radii and rich H_2/air mixtures are presented. The model (Eq. 5) describes the spherical flame propagation in good agreement for H_2-concentrations of 36.4 and 43.3 % H_2 in air and radii of 4.18 m and 2.7 m. Furthermore, the large scale experiments with stoichiometric H_2/air-mixtures presented in [9] show good agreement with the model up to a radius of 1m. In this example the flame acceleration decays at a radius of 0.8 m, while the model (Eq. 5) shows a constant acceleration.

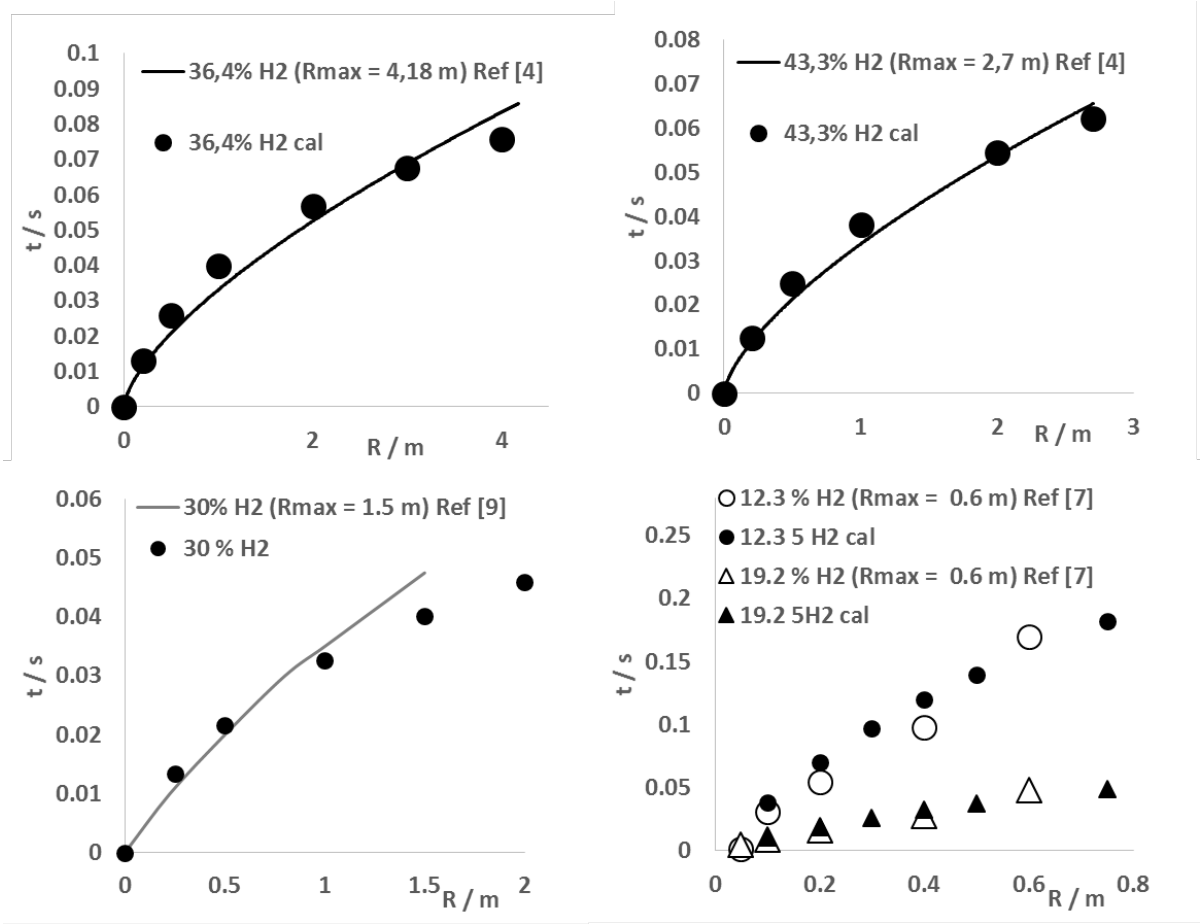

Fig. 13: Comparison of the model (Eq. 5) with other data for unconfined spherical flame propagation.

5.0 SUMMARY AND CONCLUSIONS

This work investigates the unconfined spherical and semi confined cylindrical flame propagation for H_2/air mixtures. A large scale shadowgraphy set-up for high speed applications was used to produce high quality images, allowing detailed measurements of the flame propagation velocity up to a flame radius of 0.5 m. The flame propagation was investigated in a facility consisting of two transparent solid walls with 1 m^2 area and four weak side walls made from thin plastic film. The gap size between the solid walls has been varied stepwise from a thin layer geometry (6 mm) to cube geometry (1 m). The rate of spherical flame acceleration was found to be linear and specific for each H_2/air mixture. A characteristic spherical burning velocity $S_{(sph)}$ for undisturbed spherical flame propagation was derived from the experimental data. Based on this H_2-concentration-characteristic spherical burning velocity $S_{(sph)}$ a model was formulated to determine the visible unconfined spherical flame propagation for a wide range of H_2/air mixtures. The model is in good agreement with other experimental data for large scale spherical flame propagation in H_2/air mixtures. The model is also able to describe the flame propagation in cylindrical H_2/air mixtures for the investigated gap sizes from 6 mm up to 100 mm up to a "critical" radius. Beyond this radius the model fails potentially because of the increasing overpressure. The overpressure which corresponds to the beginning of the deviation is in the range of 10 mbar. It is assumed that at this point other flame instability mechanisms, which are not included in the characteristic spherical burning velocity $S_{(sph)}$, play a dominant role in the flame propagation. The effect of self-acceleration of the burning velocity of H_2/air mixtures should be considered during the modeling of explosion hazards.

REFERENCES.

1. Darrieus G. unpublished work presented at La Technique Moderne, and at Le Congres de Mecanique Appliquee, 1945 and 1938.
2. Landau LD. On the theory of slow combustion. Acta Physicochim 1944;19(No. 1):77e85.
3. Bradley D, Cresswell TM, Puttock JS. Flame acceleration due to flame-induced instabilities in large-scale explosions. Combust Flame 2001;124(No. 4):551e9.
4. Gostintsev YA, Istratov AG, Shulenin YV. Self-similar propagation of a free turbulent flame in mixed gas mixtures, Combustion. Explos Shock Waves 1988;24(No. 5):563e9.
5. Gostintsev YA, Fortov VE, Shatskikh YV. Self-similar propagation law and fractal structure of the surface of a free expanding turbulent spherical flame. Dokl Phys Chem 2004;397(No. 1):141e4.
6. Bauwens CR, Bergthorson JM, Dorofeev SB. Experimental study of spherical-flame acceleration mechanisms in largescale propaneeair flames. Proc Combust Inst 2015;35(No. 2):2059e66.
7. Bauwens CRL, Bergthorson JM, Dorofeev SB. Experimental investigation of spherical-flame acceleration in lean hydrogen-air mixtures. Int J Hydrogen Energy 2017;42:7691 e7.
8. Kuznetsov M, Kobelt. S, Grune J, Jordan T, Flammability limits and laminar flame speed of hydrogeneair mixtures at sub-atmospheric pressures, International Journal of Hydrogen Energy (2012), http://dx.doi.org/10.1016/j.ijhydene.2012.05.049
9. Kim, W.K., Mogi, T., Kuwana, K. and Dobashi, R., Self-similar propagation of expanding spherical flames in large scale gas explosions, Proceedings of the Combustion Institute, 35, No. 2, 2015, pp. 2051-2058.
10. Yanez J, Kuznetsov M, Grune J., Combust. Flame (2015), http://dx.doi.org/10.1016/ j.combustflame. 2015.04.004